18th International Conference on Information Fusion
Washington, DC - July 6-9, 2015

Information Weighted Consensus-based Cooperative Space Object Tracking to overcome Malfunctioned Sensors and Noisy Links

Bin Jia, Khanh D. Pham, Erik Blasch, Dan Shen, Zhonghai Wang, Xin Tian, and Genshe Chen

***Abstract*—With the rapid development of sensor technology, multiple sensors are often available in many engineering applications, such as space object tracking. How to effectively use multiple sensor information is the key to achieving accurate space object state information. In this paper, the information weighted consensus (IWC) strategy is deployed to solve the cooperative sensor tracking problem. In addition, the information theoretic method and the repeated consensus, are used to detect a malfunctioned sensor and overcome the problem of noisy links in the cooperative tracking scenario. The proposed algorithms are demonstrated by a typical space object tracking problem using multiple sensors. The results indicate that: 1) The proposed algorithms can obtain stable estimation results when there is malfunctioned node in the network, 2) can mitigate the effect of noisy links, and 3) achieves close performance to the result with perfect communication links and known malfunctioned node. The results will facilitate the application of using the information weighted consensus algorithm for real multiple sensor space object tracking scenarios.**

***Index Terms*—Consensus, Kalman filter, Space object tracking, Cubature rule, Malfunctioned node, Noisy links, Space situational awareness.**

I. INTRODUCTION

MULTIPLE sensors are dedicated to achieving space situational awareness (SSA). In this paper, we propose a space object tracking algorithm using multiple sensors with the consideration of malfunctioned nodes and noisy links. For the multiple sensor tracking, there are two typical ways to use the information from multiple sensors, the centralized approach and distributed approach. In this paper, we mainly focus on the distributed cooperative tracking scenario due to the fact that distributed information fusion is more robust than the centralized information fusion.

Distributed cooperative tracking has been intensively researched and there are many different strategies, such as gossip [1], consensus [2, 3], and diffusion [4]. Specifically, the information weighted consensus strategy [5] is used due to its simplicity to implement and high accuracy. One critical issue for the distributed cooperative tracking algorithm is that some sensors may be malfunctioning and/or the communications links are often noisy. Hence, a malfunctioned node detection algorithm is required for the accurate SSA. In this paper, we propose using the information theoretic method to detect the malfunctioned node and repeated consensus to mitigate the effect of the communication noises.

In this paper, we assume that it is known that the data from the different sensors pertain to the same target. If that is not the case, track to track fusion algorithms [6-10], such as cross-covariance [6], covariance intersection [8], and covariance union [9], should be used. In addition, when multiple measurements of multiple targets are available, the data association [10] should be performed. In this paper, we only focus on the single target tracking problem with multiple synchronized measurements. Due to the popularity of the derivative free filters [11-17], in this paper, we assumed that the system is a Gaussian nonlinear system. The result, however, can be immediately extended to the non-Gaussian nonlinear system by using the Gaussian mixture Kalman filtering framework.

The remainder of the paper is organized as follows. The space object tracking problem using multiple sensors is introduced in Section II. Section III introduces the centralized multiple sensor estimation. Section IV introduces cubature rule embedded distributed multiple sensor estimation for malfunctioned node detection as well as communication noise mitigation. A multiple sensor space object tracking scenario is used and results are shown in Section V. Section VI gives the concluding remarks.

II. PROBLEM STATEMENT

A. Dynamic equation

The dynamic equation of the near-earth space object is given by [18]

$$\ddot{\mathbf{r}} = -\frac{\mu}{r^3}\mathbf{r} + \mathbf{a}_{J_2} + \mathbf{v} \tag{1}$$

Bin Jia is with the Intelligent Fusion Technology, Inc. 20271 Goldenrod Lane, Suite 2066 Germantown, MD 20876 (e-mail:bin.jia@intfusiontech.com).
Khanh D. Pham is with Space Vehicles Directorate, Air Force Research Lab, Kirtland AFB, NM 87117 (email: khanh.pham.1@us.af.mil).
Erik Blasch is with Information Directorate, Air Force Research Lab, Rome, NY 13441 (email: erik.blasch.1@us.af.mil).
Dan Shen, Zhonghai Wang, Xin Tian, Genshe Chen are with the Intelligent Fusion Technology, Inc. 20271 Goldenrod Lane, Suite 2066 Germantown, MD 20876 USA (e-mail: {dshen,zwang, xtian, gchen}@intfusiontech.com).

where $\mathbf{r}=[x,y,z]^T$ is the position of the object in the inertial coordinate frame (I-J-K), μ is the standard gravitational constant, $r=\sqrt{x^2+y^2+z^2}$, $\mathbf{a}_{J_2}$ is the $J2$ perturbations, and $\mathbf{v}$ is the white Gaussian process noise.

$$\mathbf{a}_{J_2}=-\frac{3}{2}J_2\left(\frac{R_E}{r}\right)^2\cdot\left[x\left(5\frac{z^2}{r^2}-1\right),y\left(5\frac{z^2}{r^2}-1\right),z\left(5\frac{z^2}{r^2}-3\right)\right]^T \quad (2)$$

where R_E is the radius of the earth and J_2 is a constant.

B. Space Based Optical (SBO) Sensors

The SBO uses the Photogrammetry technique to determine the position of the object [19]. By using the pointing information of an SBO sensor, the beginning and ending points of the streaks detected on the focal plane can be transformed into two angular measurements [19, 20]. In this paper, we use the azimuth and elevation as the measurements of the SBO; e.g.,

$$\begin{cases} az=\tan^{-1}\left(\dfrac{y-y_i}{x-x_i}\right)+n_1 \\ el=\tan^{-1}\left(\dfrac{z-z_i}{\sqrt{(x-x_i)^2+(y-y_i)^2}}\right)+n_2 \end{cases} \quad (3)$$

where $[x_i,y_i,z_i]^T$ is the position of the ith SBO and $\mathbf{n}=[n_1,n_2]$ is the measurement noise.

Measurements from the ith observer will be unavailable when the line-of-sight path between the observer and the space object is blocked by the Earth. The condition of the Earth blockage is examined between the distance function D and the radius of the Earth R_E. If there exist $\theta\in[0,1]$ such that $D_\theta(i)<R_E$, where

$$D_\theta(i)=\sqrt{[(1-\theta)x_i+\theta x]^2+[(1-\theta)y_i+\theta y]^2+[(1-\theta)z_i+\theta z]^2}. \quad (4)$$

then the measurement from the ith sensor to the target will be unavailable. The minimum of $D_\theta(i)$ is achieved at $\theta=\theta^*$, where θ^* is given by

$$\theta^*=-\frac{x_i(x-x_i)+y_i(y-y_i)+z_i(z-z_i)}{(x-x_i)^2+(y-y_i)^2+(z-z_i)^2} \quad (5)$$

Thus, we first examine whether $\theta^*\in[0,1]$ and then check the Earth blockage condition $D_{\theta^*}(i)<R_E$.

Besides Earth blockage, imaging quality of the SBO highly depends on the geometric relation of the space object, the SBO, and the sun as shown in Figure 1.

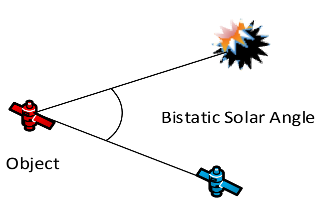

Figure 1. Bistatic solar angle illustration

We define the bistatic solar angle α as the angle of the line from the space object to the sun and the line from the object to the SBO. The lighting condition is strong when the angle is small and it is weak when the angle α is large. When α is large, the space object is hard to be observed due to saturation. When the epoch of the simulation is given, the position of the sun in Earth-centered inertial (ECI) coordinate system is denoted by $\mathbf{x}_s=[x_s,y_s,z_s]^T$. Similarly, the position of the SBO and the space object in ECI coordinates, denoted by $\mathbf{x}_m=[x_m,y_m,z_m]^T$ and $\mathbf{x}_o=[x_o,y_o,z_o]^T$ respectively, can also be obtained. By the law of cosines, the bistatic solar angle α is given by

$$\alpha=\cos^{-1}\left(\frac{D_{os}^2+D_{om}^2-D_{ms}^2}{2D_{os}D_{om}}\right) \quad (6)$$

where $D_{os}=\|\mathbf{x}_o-\mathbf{x}_s\|_2$, $D_{om}=\|\mathbf{x}_o-\mathbf{x}_m\|_2$, and $D_{ms}=\|\mathbf{x}_m-\mathbf{x}_s\|_2$.

As the light quality depends on the value of the bistatic solar angle, the measurement noise in Eq. (3) is quantized for different bistatic solar angles. We list the relation between bistatic solar angle, light quality, and the noise covariance, **R**, in Table I.

TABLE I, RELATION BETWEEN BISTATIC SOLAR ANGLE AND LIGHT

Bistatic Solar Angle (degree)	Light Quality	Noise Covariance
0-20	Excellent	0.8 **R**
20-40	Very Good	0.9 **R**
40-60	Good	1 **R**
60-75	Medium	1.1 **R**
75-90	Fair	1.2 **R**

Note that, the **R** used in Table I is a reference covariance which is set to $diag\left([4\text{arc sec},4\text{arc sec}]^2\right)$. The covariance values in Table 1 will be used in the simulation scenarios. When the bistatic solar angle is greater than 90 degrees, it is assumed that no useful measurement can be obtained. The assumption is based on the fact that SBOs can get measurements when the bistatic solar angle is less than 100 degrees [19].

C. Ground Based Radar

A Ground radar is considered in this paper and the measurement is given by.

$$\begin{aligned} az&=\tan^{-1}(\rho_e/\rho_n)+n_{az} \\ el&=\tan^{-1}\left(\rho_u\Big/\sqrt{\rho_e^2+\rho_n^2}\right)+n_{el} \\ \|\boldsymbol{\rho}\|&=\sqrt{\rho_u^2+\rho_e^2+\rho_n^2}+n_\rho \end{aligned} \quad (7)$$

where the azimuth (az), the elevation (el), and the range $\boldsymbol{\rho}=[\rho_u,\rho_e,\rho_n]^T$ can be measured by radar site on the ground with respect to the local observer coordinate system, ($\hat{\mathbf{u}}-\hat{\mathbf{e}}-\hat{\mathbf{n}}$; "up, east, and north"). Note that the covariance of measurement noise is given by $\mathrm{diag}\left(\left[0.015^{\circ}, 0.015^{\circ}, 0.025\mathrm{km}\right]^2\right)$.

The geometry of the observation model is shown in Figure 2. The range can be related to the position vector in the inertial frame (**I**-**J**-**K**) by the coordinate transformation given by

$$\begin{bmatrix}\rho_u\\ \rho_e\\ \rho_n\end{bmatrix}=\begin{bmatrix}\cos\lambda & 0 & \sin\lambda\\ 0 & 1 & 0\\ -\sin\lambda & 0 & \cos\lambda\end{bmatrix}\begin{bmatrix}\cos\theta & \sin\theta & 0\\ -\sin\theta & \cos\theta & 0\\ 0 & 0 & 1\end{bmatrix}\begin{bmatrix}x-\|\mathbf{R}\|\cos\lambda\cos\theta\\ y-\|\mathbf{R}\|\cos\lambda\sin\theta\\ z-\|\mathbf{R}\|\sin\lambda\end{bmatrix} \quad (8)$$

where $\|\mathbf{R}\|=6378.1363\,\mathrm{km}$ is the Earth radius; λ and θ are the latitude and local sidereal time of the observer respectively; and n_{az}, n_{el}, n_ρ are the white Gaussian measurement noise.

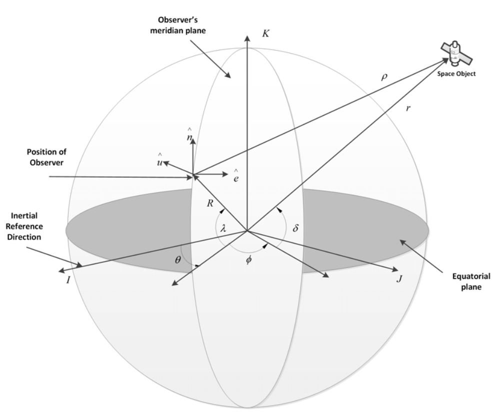

Figure 2. Illustration of the observing geometry

III. Centralized Multiple Sensor Estimation

Considering a class of nonlinear discrete-time dynamical systems

$$\mathbf{x}_k = \boldsymbol{f}\left(\mathbf{x}_{k-1}\right)+\mathbf{v}_{k-1} \quad (9)$$

$$\mathbf{z}_{k,j} = \boldsymbol{h}_j\left(x_k\right)+\boldsymbol{n}_{k,j} \quad (10)$$

where $\mathbf{x}_k \in \mathbf{R}^n; \mathbf{z}_{k,j} \in \mathbf{R}^m$. $\boldsymbol{v}_{k-1}$ and $\boldsymbol{n}_{k,j}$ are independent white Gaussian process noise and measurement noise with covariance $\mathbf{Q}_{k-1}$ and $\mathbf{R}_{k,j}$, respectively. $\mathbf{z}_{k,j}$ is the measurement by the j^{th} sensor, $j=1,\cdots,N_{sn}$ and N_{sn} is the number of sensors.

For the centralized fusion methods, the information filter is commonly used due to its simplicity for multiple sensor applications [21-23]. In the information filter, the information state and the information matrix at time $k-1$ are defined by $\hat{\mathbf{y}}_{k-1|k-1} = \mathbf{P}_{k-1|k-1}^{-1}\hat{\mathbf{x}}_{k-1|k-1}$ and $\mathbf{Y}_{k-1|k-1} = \mathbf{P}_{k-1|k-1}^{-1}$, respectively. The system state $\hat{\mathbf{x}}_{k-1|k-1}$ and covariance $\mathbf{P}_{k-1|k-1}$ can be obtained by $\hat{\mathbf{x}}_{k-1|k-1} = \mathbf{P}_{k-1|k-1}\hat{\mathbf{y}}_{k-1|k-1}$ and $\mathbf{P}_{k-1|k-1} = \mathbf{Y}_{k-1|k-1}^{-1}$, respectively. In the following, the extended information filter is introduced.

The centralized extended information filter (CEIF) is derived from the EKF and contains the prediction and update steps:

A. Prediction

The information state $\hat{\mathbf{y}}_{k|k-1}$ and the information matrix $\mathbf{Y}_{k|k-1}$ can be predicted by

$$\hat{\mathbf{y}}_{k|k-1} = \mathbf{P}_{k|k-1}^{-1}\hat{\mathbf{x}}_{k|k-1} \quad (11)$$

$$\mathbf{Y}_{k|k-1} = \mathbf{P}_{k|k-1}^{-1} \quad (12)$$

The predicted state and the associated covariance matrix at time k can be obtained by $\hat{\mathbf{x}}_{k|k-1} = \boldsymbol{f}\left(\hat{\mathbf{x}}_{k-1|k-1}\right)$ (13)

$$\mathbf{P}_{k|k-1}=\mathbf{F}_{k|k-1}\mathbf{P}_{k-1|k-1}\mathbf{F}_{k|k-1}^T+\mathbf{Q}_{k-1} \quad (14)$$

where $\mathbf{F}_{k|k-1}$ is the Jacobian matrix of $\boldsymbol{f}$ with respect to $\hat{\mathbf{x}}_{k|k-1}$.

B. Update

For multiple sensor estimation, the information state and the information matrix can be updated by [21]

$$\hat{\mathbf{y}}_{k|k} = \hat{\mathbf{y}}_{k|k-1} + \sum_{j=1}^{N_{sn}}\mathbf{i}_{k,j} \quad (15)$$

$$\mathbf{Y}_{k|k} = \mathbf{Y}_{k|k-1} + \sum_{j=1}^{N_{sn}}\mathbf{I}_{k,j} \quad (16)$$

where the information state contribution $\mathbf{i}_{k,j}$ and the information matrix contribution $\mathbf{I}_{k,j}$ of the j^{th} sensor are given by

$$\mathbf{i}_{k,j}=\mathbf{H}_{k,j}^T\mathbf{R}_{k,j}^{-1}\left[\left(\mathbf{z}_{k,j}-\boldsymbol{h}_j\left(\hat{\mathbf{x}}_{k|k-1}\right)\right)+\mathbf{H}_{k,j}\hat{\mathbf{x}}_{k|k-1}\right] \quad (17)$$

$$\mathbf{I}_{k,j} = \mathbf{H}_{k,j}^T\mathbf{R}_{k,j}^{-1}\mathbf{H}_{k,j} \quad (18)$$

where $\boldsymbol{h}_j$ and $\mathbf{H}_{k,j}$ are the j^{th} measurement function and the associated Jacobian matrix at time k, respectively; $\mathbf{R}_{k,j}$ is the covariance of the measurement noise corresponding to the j^{th} measurement equation.

Remark 2.1: From the above CEIF filtering algorithm, it can be seen that the local information contributions of $\mathbf{i}_{k,j}$ and $\mathbf{I}_{k,j}$ are only computed at sensor j and the total information contribution. Therefore, the information filter is computationally more efficient and more suitable for decentralized sensor estimation than the conventional Kalman filter.

The centralized cubature information filter (CCIF) can be obtained by integrating the cubature rule with the framework of CEIF. More details can be found in [21, 22].

IV. Distributed Multiple Sensor Estimation

For the distributed fusion algorithm, the network topology should first be provided and it can be represented by an undirected connected graph $G=(V,E)$, where V is the set of vertices or nodes of the graph and E is the set of edges or lines of the graph. Before the introduction of the distributed cooperative tracking algorithm, the average consensus algorithm is briefly introduced as follows since it is the fundamental component of the consensus-based estimation algorithms.

A. Average Consensus Algorithm

The average consensus algorithm is frequently used to obtain the mean value of all nodes in the network. Given the value of each node, the set of values of the network can be represented by $\left\{a_j\right\}_{j=1}^{N_{sn}}$. By using the average consensus algorithm, the mean value $\frac{1}{N_{sn}}\sum_{j=1}^{N_{sn}} a_j$ can be obtained by multiple iterations. The value of each node is initialized by $a_j(0)=a_j$ and iterative change values with its neighbors and updates to its own value. We assume that the each node has the value $a_j(i-1)$ before exchanging the values at iteration step i, then the jth node exchange the values with its neighbors $j' \in N_j$, which means the jth node sends its value to its neighbors and also receives neighbors' values $a_{j'}(i-1)$. Note N_j denotes the set of nodes which connect with node j. The update stage of the jth node value from $(i$-1$)$-th iteration to i-th iteration is given by

$$a_j(i)=a_j(i-1)+\varepsilon\sum_{j'\in N_j}\left(a_{j'}(i-1)-a_j(i-1)\right) \tag{19}$$

where ε is the rate parameter which is a value between 0 and $1/\Delta_{\max}$, and $\Delta_{\max}$ is the maximum degree of the network. Note that the convergence will be faster if a large ε is chosen.

B. Information Weighted Consensus Filter

The prediction step of the information weighted consensus filter (IWCF) is identical to that of CEIF since the prediction step at each sensor is the same. The update step of the IWCF, by Eqs. (11)-(16), can be written as

$$\begin{aligned}\hat{\mathbf{x}}_{k|k} &= \left(\mathbf{Y}_{k|k}\right)^{-1}\left(\hat{\mathbf{y}}_{k|k}\right)=\left(\mathbf{Y}_{k|k-1}+\sum_{j=1}^{N_{sn}}\mathbf{I}_{k,j}\right)^{-1}\left(\hat{\mathbf{y}}_{k|k-1}+\sum_{j=1}^{N_{sn}}\mathbf{i}_{k,j}\right)\\ &=\left(\sum_{j=1}^{N_{sn}}\left(\frac{\mathbf{Y}_{k|k-1}}{N_{sn}}+\mathbf{I}_{k,j}\right)\right)^{-1}\left(\sum_{j=1}^{N_{sn}}\left(\frac{\hat{\mathbf{y}}_{k|k-1}}{N_{sn}}+\mathbf{i}_{k,j}\right)\right)\end{aligned} \tag{20}$$

and
$$\mathbf{Y}_{k|k}=\sum_{j=1}^{N_{sn}}\left(\frac{\mathbf{Y}_{k|k-1}}{N_{sn}}+\mathbf{I}_{k,j}\right). \tag{21}$$

For the IWCF, it is assumed that *a priori* information for each node is the same. Under this assumption, we have $\hat{\mathbf{x}}_{k|k-1,j}=\hat{\mathbf{x}}_{k|k-1}$. Then, Eq. (20) can be rewritten as

$$\hat{\mathbf{x}}_{k|k}=\left(\sum_{j=1}^{N_{sn}}\left(\frac{\mathbf{Y}_{k|k-1,j}}{N_{sn}}+\mathbf{I}_{k,j}\right)\right)^{-1}\left(\sum_{j=1}^{N_{sn}}\left(\frac{\hat{\mathbf{y}}_{k|k-1,j}}{N_{sn}}+\mathbf{i}_{k,j}\right)\right) \tag{22}$$

and
$$\mathbf{Y}_{k|k}=\sum_{j=1}^{N_{sn}}\left(\frac{\mathbf{Y}_{k|k-1,j}}{N_{sn}}+\mathbf{I}_{k,j}\right) \tag{23}$$

Define the terms $\mathbf{V}=\frac{\mathbf{Y}}{N_{sn}}+\mathbf{I}$, $\mathbf{v}=\frac{\mathbf{Y}}{N_{sn}}\mathbf{x}+\mathbf{i}$; and let $\mathbf{V}_j(0)=\frac{\mathbf{Y}_j}{N_{sn}}+\mathbf{I}_j$, $\mathbf{v}_j(0)=\frac{\mathbf{Y}_j}{N_{sn}}\mathbf{x}_j+\mathbf{i}_j$, by using the average consensus algorithm. When the iteration number goes infinity, we have

$$\lim_{i\to\infty}\mathbf{V}_j(i)=\frac{\sum_{j=1}^{N_{sn}}\mathbf{V}_j(0)}{N_{sn}} \tag{24}$$

and
$$\lim_{i\to\infty}\mathbf{v}_j(i)=\frac{\sum_{j=1}^{N_{sn}}\mathbf{v}_j(0)}{N_{sn}} \tag{25}$$

Hence, the update equations are given by

$$\begin{aligned}\hat{\mathbf{x}}_{k|k} &=\left(\sum_{j=1}^{N_{sn}}\left(\frac{\mathbf{Y}_{k|k-1,j}}{N_{sn}}+\mathbf{I}_{k,j}\right)\right)^{-1}\left(\sum_{j=1}^{N_{sn}}\left(\frac{\hat{\mathbf{y}}_{k|k-1,j}}{N_{sn}}+\mathbf{i}_{k,j}\right)\right)\\ &=\lim_{i\to\infty}\left(N_{sn}\mathbf{V}_j(i)\right)^{-1}\left(N_{sn}\mathbf{v}_j(i)\right)\\ &=\lim_{i\to\infty}\left(\mathbf{V}_j(i)\right)^{-1}\left(\mathbf{v}_j(i)\right)\end{aligned} \tag{26}$$

and
$$\mathbf{Y}_{k|k}=\lim_{i\to\infty}N\mathbf{V}_j(i) \tag{27}$$

Remark 3.1, For real applications, the iteration step number i cannot be infinity, as the maximum iteration number has to be given for finite time.

C. Malfunctioned node detection

By equations (22) and (23), the information required to be exchanged between different nodes are $\mathbf{V}=\frac{\mathbf{Y}}{N_{sn}}+\mathbf{I}$ and $\mathbf{v}=\frac{\mathbf{Y}}{N_{sn}}\mathbf{x}+\mathbf{i}$. Now we assume the sensor j_1 receives information from the sensor j_2. By using the self-information, the state estimation at sensor j_1 can be given by

$$\hat{\mathbf{x}}_{k|k,j_1}=\left(\mathbf{Y}_{k|k,j_1}\right)^{-1}\left(\hat{\mathbf{y}}_{k|k,j_1}\right)=\left(\mathbf{Y}_{k|k-1}+\mathbf{I}_{k,j_1}\right)^{-1}\left(\hat{\mathbf{y}}_{k|k-1}+\mathbf{i}_{k,j_1}\right) \tag{28}$$

$$\mathbf{Y}_{k|k,j_1}=\mathbf{Y}_{k|k-1}+\mathbf{I}_{k,j_1} \tag{29}$$

where $\mathbf{i}_{k,j_1}$ and $\mathbf{I}_{k,j_1}$ can be obtained respectively by

$$\mathbf{i}_{k,j_1}=\mathbf{v}_{k,j_1}-\frac{\mathbf{Y}_{k|k-1}}{N_{sn}}\mathbf{x}_{k|k-1} \tag{30}$$

and
$$\mathbf{I}_{k,j_1}=\mathbf{V}_{k,j_1}-\frac{\mathbf{Y}_{k|k-1}}{N_{sn}} \tag{31}$$

Note that $\mathbf{x}_{k|k-1}$ and $\mathbf{Y}_{k|k-1}$ are *a priori* information.

In summary, the self-estimation of the state is described by the probability density function (PDF) $p_1=N\left(\hat{\mathbf{x}}_{k|k,j_1},\left(\mathbf{Y}_{k|k,j_1}\right)^{-1}\right)$. When the sensor receives the information from sensor j_2, the estimation using information from j_2 can be described by the PDF $\hat{p}_1=N\left(\hat{\mathbf{x}}_{k|k,j_2},\left(\mathbf{Y}_{k|k,j_2}\right)^{-1}\right)$, where,

$$\hat{\mathbf{x}}_{k|k,j_2}=\left(\mathbf{Y}_{k|k,j_2}\right)^{-1}\left(\hat{\mathbf{y}}_{k|k,j_2}\right)=\left(\mathbf{Y}_{k|k-1}+\mathbf{I}_{k,j_2}\right)^{-1}\left(\hat{\mathbf{y}}_{k|k-1}+\mathbf{i}_{k,j_2}\right) \tag{32}$$

$$\mathbf{Y}_{k|k,j_2} = \mathbf{Y}_{k|k-1} + \mathbf{I}_{k,j_2} \qquad (33)$$

The distance between p_1 and $\hat{p}_1$ can be used to detect the malfunctioned node. Specifically, if the distance between p_1 and $\hat{p}_1$ is larger than the threshold, node j_2 is declared as a malfunctioned node. Otherwise, the node j_2 is declared as a normal node. There are many methods to evaluate the distance between two pdfs, such as Kullback-Leibler (KL) divergence and Bhattacharyya divergence. However, the divergence is generally not symmetric. Hence, they generally do not satisfy the triangle inequality which is required by a metric. In this paper, the metric used to evaluate the distance between two PDFs is given [24]

$$D\left(p_1(\mathbf{x}), \hat{p}_1(\mathbf{x})\right) = \left(\mathbf{u}^T \mathbf{\Gamma}^{-1} \mathbf{u}\right)^{-\frac{1}{2}} + \left(\sum_{j=1}^{n} \log^2 \lambda_j\right)^{\frac{1}{2}} \qquad (34)$$

where

$\mathbf{u} = \hat{\mathbf{x}}_{k|k,j_1} - \hat{\mathbf{x}}_{k|k,j_2}$ and $\mathbf{\Gamma} = \frac{1}{2}\left(\left(\mathbf{Y}_{k|k,j_1}\right)^{-1} + \left(\mathbf{Y}_{k|k,j_2}\right)^{-1}\right)$.

Note that λ_j $1 \le j \le n$ is the eigenvalue by solving the equation $\left(\mathbf{Y}_{k|k,j_1}\right)^{-1} \mathbf{V} = \Lambda \left(\mathbf{Y}_{k|k,j_2}\right)^{-1} \mathbf{V}$ where $\mathbf{V}$ is the column matrix of the generalized eigenvectors and Λ is the diagonal matrix and each element of it is the eigenvalue.

Remark 3.2, In order to guarantee the correctness of self-estimation of the state, the likelihood of the self-estimation state should be evaluated. If the self-estimation is not incorrect, the information sent by the node will not be used by other nodes.

Remark 3.3 the square root of the Jensen-Shannon divergence can also be used as a metric to evaluate the distance between different PDFs. However, it has a considerably high computational load [24].

Note that when the malfunctioned node is found at time *k*, it will be excluded from the consensus procedure in the current time *k*.

D. Detect the number of normal nodes

One assumption of the ordinary IWCF is that the number of sensors can be exactly obtained. Due to the existence of the malfunctioned node, the number of sensors N_{sn} used in the ordinary IWCF is actually larger than the true number of valid sensors. Hence, the correct number of normal nodes has to be determined. We use the following protocol to determine the number of normal nodes. Before the consensus procedure at each update step, let one node exchange value 1 and other nodes exchange value 0 with their neighbor. After sufficient iterations, all nodes have the same value, i.e., $1/\overline{N}_{sn}$, where $\overline{N}_{sn}$ is the correct number of normal nodes and it can be used in the IWCF (rather than N_{sn}). Note that round operation may be required to make the number of sensors to be an integer.

E. IWCF via noisy link

The communication links between different nodes can be corrupted by noise. In order to mitigate the effect of large noise, the repeated consensus is utilized [25]. Define $\mathbf{x}_n^s(i)$ as the local value at sensor *n* and at the *i*th iteration of the *s*th Monte Carlo run. The consensus value will be calculated by

$$\overline{\mathbf{x}}_n^p(i) = \frac{1}{p}\sum_{s=1}^{p} \mathbf{x}_n^s(i) \qquad (35)$$

where *p* is the number of Monte Carlo runs. With the increasing of the repeated times p, the averaging procedure will take advantage of the law of large numbers to work effectively [25].

V. Simulation Results

To test the performance of the proposed IWCF in the presence of malfunctioned nodes and noisy links, we evaluate the performance of different filters in a cooperative space object tracking scenario. Five sensors, including one ground radar and four SBOs {SBO1, .., SBO4} are used in the scenario. The parameters of the sensors and the space object are listed in Table II. We assumed that SBO2 is a malfunctioned node and incorrect information will be sent from SBO2 randomly. In this paper, we assume the incorrect information follows a Gaussian distribution. Note that the two terms, $\mathbf{v}$ and $\mathbf{V}$ are exchanged by different nodes. For the incorrect information $\mathbf{v}$ and $\mathbf{V}$, each element x in $\mathbf{v}$ or the diagonal element of $\mathbf{V}$ is perturbed by a Gaussian noise from a Gaussian distribution $N(0, 0.1x)$.

Table II. Parameters of sensors and space object

Sensors	Initial orbital parameters/Locations
SBO1	$\mathbf{x}_{pos} = [-328.30,\text{-}791.22,6949.01]^T\ km$ $\mathbf{x}_{vel} = [-4.4652,6.0572,0.4849]^T\ km/s$
SBO2	$\mathbf{x}_{pos} = [-4143.79,5624.26,441.55]^T\ km$ $\mathbf{x}_{vel} = [0.3559,0.8495,\text{-}7.4934]^T\ km/s$
SBO3	$\mathbf{x}_{pos} = [328.29,791.24,-6949.05]^T\ km$ $\mathbf{x}_{vel} = [4.4652,-6.0571,-0.4851]^T\ km/s$
SBO4	$\mathbf{x}_{pos} = [4007.58,-5016.32,-2791.95]^T\ km$ $\mathbf{x}_{vel} = [1.1976,-2.8768,6.8769]^T\ km/s$
Radar	Latitude: 8.724 N, Longitude: 167.717 E
Initial Space Object	$\mathbf{x}_{pos} = [-1873.14,33018.75,1153.04]^T\ km$ $\mathbf{x}_{vel} = [-3.4651,-0.1963,\text{-}0.0069]^T\ km/s$

The topology of the sensor network is described by

$$E = \begin{bmatrix} 0 & 1 & 0 & 0 & 1 \\ 1 & 0 & 1 & 0 & 0 \\ 0 & 1 & 0 & 1 & 0 \\ 0 & 0 & 1 & 0 & 1 \\ 1 & 0 & 0 & 1 & 0 \end{bmatrix} \quad (36)$$

The adaptive step size Runge-Kutta method is used to propagate the orbit (Eq. (1)) and the measurement period is 60 seconds. The channel noise covariance for each state is assumed to be 1e-10. As shown in Eq. (19), the average consensus algorithm used the information difference between different nodes to update the local information. The information difference, however, sometime is very small. Hence, it is vulnerable to the noise. In addition, the signal-to-noise ratio (SNR) of the channel is reflected in the uncertainties selected for the model which include background noise, signal bias, and effects from the environment. Six different filters are tested and the root mean square error (RMSE) is used to evaluate the performance of different filters. For convenience, we list them in table III. Note that 'Cub' in Table III denotes the cubature rule, 'IC' denotes the information correction, and 'NM' denotes the noise mitigation, 'w' and 'wo' denote 'with' and 'without', respectively. The comparison between Cub-CIF and Cub-IWCF has been reported in [23].

Table III Test filters and their properties

Filters	Properties
Cub-IWCF-Benchmark	• Given malfunctioned node (excluded), and • Perfect communication channel
Cub-IWCF	• Conventional IWCF
Cub-IWCF-woIC	• Without using the correct number of normal nodes (Information Correction), but • Using the malfunctioned node detection algorithm. • Perfect communication channel
Cub-IWCF-wIC	• Using correct number of normal nodes and • Using malfunctioned node detection algorithm. • Perfect communication channel
Cub-IWCF-wIC-woNM	• Using correct number of normal nodes and • Using malfunctioned node detection algorithm. • Noisy channel but without using the noise mitigation algorithm
Cub-IWCF-wIC-wNM	• Using malfunctioned node detection algorithm. • Noisy channel and • Using the noise mitigation algorithm

The first filter is named 'Cub-IWCF-Benchmark' in which the malfunctioned node is known and excluded from the network. In addition, the communication channel is assumed to be perfect (no noise). Cub- IWCF -Benchmark can be used as a baseline to evaluate the performance of other filters. Cub-IWCF is a conventional filter without considering the malfunctioned node. Specifically, it accepts the information from the malfunctioned node to update its estimation. In our simulations, Cub- IWCF often diverges. Hence, the results are not shown in Figures 3 and 4.

As shown in Figures 3 and 4, Cub-IWCF-woIC and Cub-IWCF-wIC are used to demonstrate the effectiveness of the malfunctioned node detection algorithm. In Cub-IWCF-woIC, the number of nodes includes the malfunctioned node. Hence, the information exchanged between different nodes is not corrected accordingly. Cub-IWCF-wIC, however, revises the information exchanged between different nodes by the correct number of normal nodes. Note that in both filers, perfect communication channels are assumed. Our simulation results show that Cub-IWCF-wIC achieved more accurate results than the Cub-IWCF-woIC. In addition, the Cub-IWCF-wIC achieved very close performance to the Cub-IWCF-Benchmark.

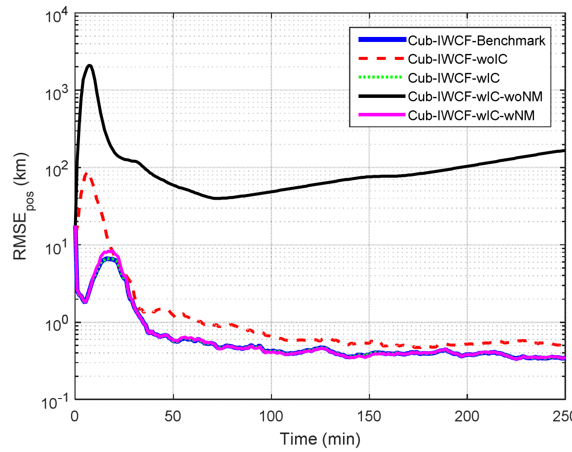

Figure 3. RMSE of position versus time

Cub-IWCF-wIC-woNM and Cub-IWCF-wIC-wNM are used to demonstrate the effectiveness of the noise mitigation algorithm for noisy links. In Cub-IWCF-wIC-woNM, the malfunctioned node detection algorithm is used and the information is corrected according to the correct number of normal nodes. However, the communication channel has noise above a threshold. Due to the effect of the noise, the estimation eventually diverges. The repeated consensus is used in Cub-IWCF-wIC-wNM which can successfully mitigate the effect of the noise and achieve satisfying results. Note that Cub-IWCF-wIC-wNM is only slightly worse than Cub-IWCF-Benchmark between time interval from 15 to 25 minutes.

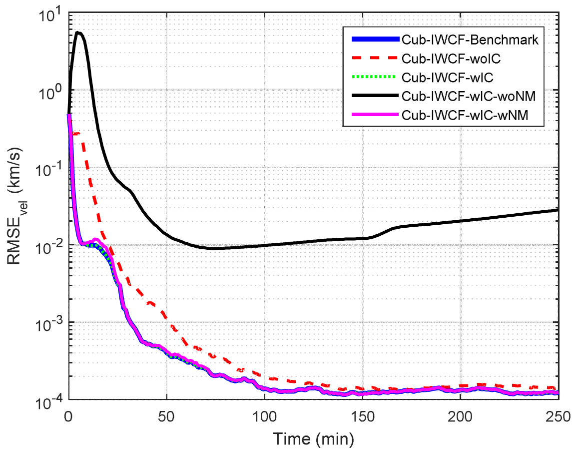

Figure 4. RMSE of velocity versus time

VI. Conclusion

Building on the consensus-based filter, an information theoretic method is proposed to detect the malfunction node and a repeated consensus algorithm is used to mitigate the effect of communication channel noise between different sensors in the cooperative space object tracking scenario. The simulation results show that the proposed strategy is effective to detect the malfunctioned node and the communication noise has been effectively mitigated by repeated consensus strategy. The result benefits the applications of space situational awareness using multiple sensors.

ACKNOWLEDGMENT

This research was partly supported by the United States Air Force under contract number FA9453-14-M-0161. The views and conclusions contained herein are those of the authors and should not be interpreted as necessarily representing the official policies or endorsements, either expressed or implied, of the United States Air Force.

References

[1] S. Kar and J.M.F. Moura, “Gossip and distributed Kalman filtering: Weak consensus under weak detectability,” *IEEE Transactions on Signal Processing, vol. 59, no. 4, pp. 1766-1784, 2011.*

[2] R. Olfati-Saber, J.A.Fax, R.M. Murray, “Consensus and cooperation in networked multi-agent systems,” *Proceedings of the IEEE*, vol. 95, no.1, 2007.

[3] R. Olfati-Saber, "Kalman-consensus filter: Optimality, stability, and performance." Decision and Control, 2009 held jointly with the 2009 28th Chinese Control Conference. CDC/CCC 2009. *Proceedings of the 48th IEEE Conference on*, 2009.

[4] F.S. Cattivelli and A. H. Sayed, “Diffusion strategies for distributed Kalman filtering and smoothing,” *IEEE Transactions on Automatic Control*, vol. 55, no. 9, 2010.

[5] K. Ahmed Tashrif, J. A. Farrell, and A. K. Roy-Chowdhury. "Information weighted consensus." *2012 IEEE Conference on Decision and Control*, 2012.

[6] Y. Bar-Shalom, “On the track-to-track correlation problem,” *IEEE Transactions on Automatic Control*, vol. AC-26, no. 2, pp.571 -572 1981

[7] K. C. Chang, R. K. Saha, Y. Bar-shalom, “On optimal track-to-track fusion,” *IEEE Transactions on Aerospace and Electronic Systems*, vol. 33, no.4, pp.1271-1276, 1997.

[8] S. J. Julier and J. K. Uhlmann, *Handbook of Data Fusion*. CRC Press, 2001, ch. 12: General decentralized data fusion with covariance intersection (CI), pp. 1–25.

[9] J. K. Uhlmann, *Dynamic map building and localization for autonomous vehicles*, Ph.D. dissertation, University of Oxford, 1995.

[10] Y. Bar-Shalom, *Multitarget/Multisensor Tracking: Applications and Advances*, Artech House Radar Library, 2000.

[11] S. J. Julier, and J. K. Uhlmann, “Unscented filtering and nonlinear estimation,” *Proceedings of the IEEE*, vol. 92, no. 3, 2004, pp. 401-422.

[12] I. Arasaratnam, and S. Haykin, “Cubature Kalman filters,” *IEEE Transactions on Automatic Control*, vol. 54, no. 6, 2009, pp. 1254-1269.

[13] B. Jia, M. Xin, and Y. Cheng, “High-degree cubature Kalman filter,” *Automatica*, vol. 49, no. 2, pp. 510-518, 2013.

[14] K. Ito and K. Xiong, “Gaussian filters for nonlinear filtering problems,” *IEEE Transactions on Automatic Control*, vol. 45, no. 5, 2000, 910-927.

[15] B. Jia, M. Xin, and Y. Cheng, “Sparse Gauss-Hermite quadrature filter with application to spacecraft attitude,” *Journal of Guidance, Control, and Dynamics*, vol. 34, no. 2, pp. 367-379.

[16] B. Jia, M. Xin, and Y. Cheng, “Sparse-grid quadrature nonlinear filtering,” *Automatica*, vol. 48, no. 2, pp. 327-341, 2012.

[17] J. Dun´ık, O. Straka, and M. ˇSimandl, “Stochastic integration filter,” *IEEE Transactions on Automatic Control,* vol. 58, no. 6, pp. 1561–1566, 2013.

[18] D. A. Vallado, *Fundamentals of astrodynamics and applications*. vol. 12. Springer, 2001.

[19] J. Sharma, *et al*., "Toward operational space-based space surveillance." *Lincoln Laboratory Journal* 13.2, pp. 309-334, 2002.

[20] G. H. Stokes, *et al*., "The space-based visible program." *Lincoln Laboratory Journal* 11.2, pp.205-238, 1998.

[21] B. Jia, X. Ming, and Y. Cheng. "Multiple sensor estimation using the sparse Gauss-Hermite quadrature information filter." *American Control Conference (ACC)*, 2012. IEEE, 2012.4

[22] B. Jia, *et al.* "Multiple sensor estimation using a high-degree cubature information filter." *Proceedings of SPIE* vol. 8739, 87390T, 2013.

[23] B. Jia, K. D. Pham, E. Blasch, D. Shen, Z. Wang, and G. Chen, “Cooperative Space Object Tracking using Consensus- based Filters,” *17th International Conference on Information Fusion*, 2014.

[24] K. T. Abou-Moustafa and F. P. Ferrie, “A note on metric properties for some divergence measures: the Gaussian case,” *Asian Conference on Machine Learning,* vol. 25, pp. 1-15, 2012.

[25] S. Kar and J. M. F. Moura, “Distributed consensus algorithms in sensor networks with imperfect communication: link failures and channel noise,” *IEEE Transactions on Signal Processing*, Vol. 57, No. 1, pp. 355-369, 2009.